COMMUNICATION

Synergistic effect of side-chain and backbone engineering in thieno[2,3-*f*]benzofuran-based conjugated polymers for high performance non-fullerene organic solar cells†

Keke Dou,‡[a] Xunchang Wang,‡[bc] Zurong Du,[bc] Huanxiang Jiang,[bc] Feng Li,[d] Mingliang Sun [ID] *[a] and Renqiang Yang [ID] *[b]

Most polymer donors developed so far for high-performance polymer solar cells (PSCs) are designed in planar molecular geometries containing benzodithiophene (BDT) units. In this study, three two-dimensional conjugated polymers, PTBF$_{EH}$-BDD, PTBFS$_{DO}$-BDD and PTBFS$_{EH}$-BDD, based on thieno[2,3-*f*]benzofuran (TBF) building blocks with different side-chains are designed and synthesized. It is found that the TBF unit can inherit and integrate the advantages of both the BDT and benzo[1,2-*b*:4,5-*b′*]difuran (BDF) building blocks. Due to the synergistic effects of oxygen and sulfur in the backbone and the optimized side chain, PTBF$_{EH}$-BDD shows a higher absorption coefficient, more suitable aggregation and improved hole mobility in comparison with PTBFS$_{DO}$-BDD and PTBFS$_{EH}$-BDD, which improves the J_{SC} and FF in PSCs. The PSCs based on PTBF$_{EH}$-BDD:ITIC achieve a power conversion efficiency (PCE) of 11.13% with a J_{SC} of 17.76 mA cm^{-2}, a V_{OC} of 0.893 V, and a FF of 70.16%, which is comparable with its BDT counterparts. Moreover, the PSCs based on these three TBF-based devices do not need any extra post treatments or additives. This study demonstrates that the TBF-based polymers are promising candidates for highly efficient non-fullerene PSCs.

Introduction

Non-fullerene polymer solar cells (PSCs), emerging as a competitive photovoltaic technology, have had tremendous progress in recent years.[1-4] Traditional non-fullerene PSCs are based on a bulk hetero junction (BHJ) structure consisting of p-type conjugated polymers as donors (D) and n-type organic small molecules such as 3,9-bis(2-methylene-(3-(1,1-dicyano-methylene)-indanone))-5,5,11,11-tetrakis(4-hexylphenyl)-dithieno[2,3-*d*:2′,3′-*d′*]-*s*-indaceno[1,2-*b*:5,6-*b′*]-dithiophene (ITIC)) as acceptors (A).[5-19] Due to the advantages of broader and more complementary absorption, easily tunable energy levels and compatible morphologies, the power conversion efficiency (PCE) for non-fullerene PSCs has already surpassed 14%.[20-25]

For the design and synthesis of new p-type conjugated polymer donor materials that would match well with the small molecule acceptor, backbone and side chain engineering are the two general methods to modify the polymers.[26-38] As for backbone engineering, precisely selecting various electron-donor and electron-acceptor moieties to construct a D–A copolymer is an effective strategy for developing high performance solar cells. Benzodithiophene (BDT), synthesized by fusing a benzene unit with two flanking thiophene units, has emerged as a star donor due to its advantages such as planar structure, high mobility and easily modifiable structure.[39] A large number of classical polymers with the BDT backbone, such as wide band-gap polymers PBDB-T and J71, and medium band-gap polymer PCE10, have been designed and widely applied in non-fullerene PSCs.[6,40,41] In addition, benzo[1,2-*b*:4,5-*b′*]difuran (BDF), a furan-based derivative, is another commonly used backbone.[42] Compared with the BDT unit, the furan-based BDF possesses some unique and particular features. The smaller atomic radius of oxygen in the furan unit can guarantee a more planar structure for charge transport.[43] In comparison, the oxygen atom with an intense electronegativity can modulate the HOMO energy level and induce stronger molecular aggregation, resulting in denser p–p* stacking.[44-47] Moreover, furan is an abundant material, which can be extracted from renewable resources. However, the photovoltaic performance of the BDF-based polymers is always lower than that of the BDT-based polymers, which is due to the unsatisfied J_{SC} and FF resulting from the strong molecular aggregation.[47] Our recent study demonstrated that polymers with moderate aggregation could be more compatible with a small molecule acceptor to form

[a]*School of Material Science and Engineering, Ocean University of China, Qingdao 266100, China. E-mail: mlsun@ouc.edu.cn*

[b]*CAS Key Laboratory of Bio-based Materials, Qingdao Institute of Bioenergy and Bioprocess Technology, Chinese Academy of Sciences, Qingdao 266101, China. E-mail: yangrq@qibebt.ac.cn*

[c]*University of Chinese Academy of Sciences, Beijing 100049, China*

[d]*Key Laboratory of Rubber-Plastics of Ministry of Education/Shandong Province, School of Polymer Science and Engineering, Qingdao University of Science & Technology, Qingdao 266042, China*

‡ Keke Dou and Xunchang Wang contributed equally to this work.

a material with excellent morphology. Therefore, modulating the aggregation property of the polymer is significant for achieving high performance.

Side chain engineering is another fundamental method for polymer modification. The size, type, topology and the distribution of the side chain attached to the polymer backbone can strongly impact the molecular weight, intermolecular interactions, charge transport and morphology of the polymer/ITIC blend films, further influencing the performance of the PSCs.[27,48–50] The optimal non-conjugated alkyl chain should be as short as possible, while ensuring sufficient solubility for processing. In most cases, a branched alkyl side chain can endow polymers with better solubility than a linear chain. But polymers with linear side chains may have more ordered structure and higher crystallinity for charge transport.[48] In addition, the introduction of a sulfur atom to the side chain could lower the HOMO level to increase the open-circuit voltage (V_{OC}).[51] Moreover, the arrangement of alkyl chains can lead to morphological changes such as domain size, aggregation and miscibility of the blending. Therefore, precisely and carefully selecting an optimized side chain to modify the polymer is very important for improving the performance of PSCs.

Thieno[2,3-f]benzofuran (TBF), an asymmetric backbone that is a hybrid of BDT and BDF units, received a scant few attempts in fullerene PSCs by Zou et al.[52,53] However, the photovoltaic performances of TBF-based devices are not competitive with those of their BDT and BDF counterparts. Up to now, although there are a few reports on the application of the TBF-based copolymers as donors in non-fullerene PSCs, we hypothesize that the TBF can inherit and integrate the advantages of both BDT and BDF backbones and can potentially be applied in non-fullerene PSCs, if we simultaneously utilize side chain and backbone engineering.[54,55] Therefore, we designed and synthesized three new 2D-conjugated polymers based on TBF backbone with different side chains and 1,3-bis(thiophen-2-yl)-5,7-bis(2-ethylhexyl)benzo[1,2-c:4,5-c′]dithiophene-4,8-dione (BDD) as the acceptor unit. The three new polymers were named PTBF$_{EH}$-BDD, PTBFS$_{DO}$-BDD and PTBFS$_{EH}$-BDD, which were obtained by palladium-catalyzed Stille polycondensation. The effect of the alkyl side chains on TBF unit on the chemical structure, optical and electrical properties, charge transport and photovoltaic performance of the copolymers were systematically studied. It was found that the asymmetric backbone caused a drastic effect on the polymer geometric configuration. The side chains of different lengths and types may affect the steric hindrance of the polymers, which can significantly influence the photophysical, electrochemical, microstructural and photovoltaic performances of the polymers.[56–58] The photovoltaic performances of all the polymers were investigated in non-fullerene PSCs, with ITIC as the electron acceptor.

As a result, PSCs with PTBF$_{EH}$-BDD, PTBFS$_{DO}$-BDD and PTBFS$_{EH}$-BDD as donor polymers exhibited PCEs of 11.13%, 10.57% and 10.23%, respectively. The results demonstrate that utilizing the synergistic effect of both side chain and backbone engineering is an effective strategy to further tune the optoelectronic properties of polymers, and that the TBF-based polymers are promising candidates for high efficiency non-fullerene PSCs.

2. Result and discussion

Synthesis and characterization

The chemical structures of the copolymers are shown in Scheme 1 and the detailed synthetic routes are shown in Scheme S1.† The molecular structures of the intermediates were confirmed by ^{1}H NMR and ^{13}C NMR spectroscopy. The polymers showed good solubility in common solvents, such as chloroform, toluene and chlorobenzene (CB), at room temperature. The number-average molecular weights (M_n) and polydispersity indices (PDI) of the three polymers were measured by gel permeation chromatography (GPC) analysis, using polystyrene as the reference and THF (40 °C) as the eluent. The M_n of the polymers PTBF$_{EH}$-BDD, PTBFS$_{DO}$-BDD and PTBFS$_{EH}$-BDD were estimated to be 62.7, 38.5 and 52.3 kDa, respectively. The thermal properties of these three polymers were investigated by thermal gravimetric analysis (TGA) under nitrogen atmosphere, as shown in Fig. S1.† The decomposition temperatures with 5% weight loss for the three new polymers are all higher than 290 °C (see Table 1), suggesting that all of the polymers possess good thermal stability that is adequate for their application in PSCs.

Optical and electrochemical properties

The normalized absorption spectra for the three polymers in both dilute chlorobenzene (CB) solutions and thin films at ambient temperature are shown in Fig. 1, and the corresponding absorption data are summarized in Table 2. As shown in Fig. 1a and b, the polymers show broad absorption from 300 to 700 nm, covering the whole visible spectrum. The absorption band region from 500–700 nm originated from the intramolecular charge transfer process from the donor segments (TBF) to the acceptor segments (BDD), and the other minor
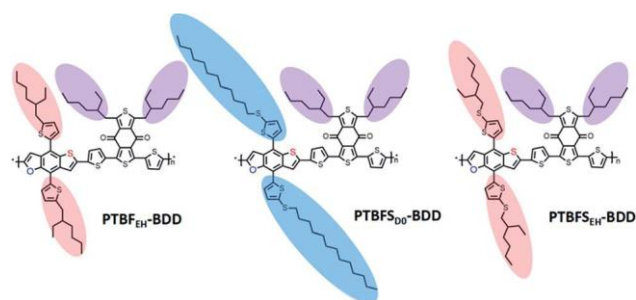
Scheme 1 The chemical structures of the three copolymers.

Table 1 Molecular weights and thermal properties of the polymers

Polymers	$M_n{}^a$ (kDa)	PDI^a	$T_d{}^b$ (°C)
PTBF$_{EH}$-BDD	62.7	1.63	365
PTBFS$_{DO}$-BDD	38.5	1.91	296
PTBFS$_{EH}$-BDD	52.3	1.58	327

^{a} Number-average molecular weights (M_n) and PDI of the polymers were determined by GPC using polystyrene standards. ^{b} 5% weight loss temperature was measured by TGA under nitrogen flow.

This journal is © The Royal Society of Chemistry 2019
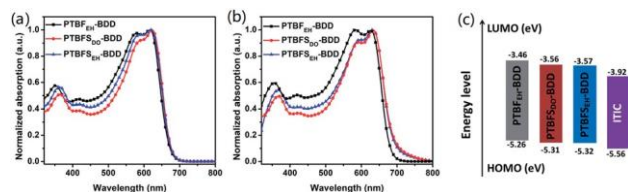
J. Mater. Chem. A, 2019, 7, 958–964 | 959

Fig. 1 Normalized UV-vis absorption spectra of the polymers in (a) chloroform solutions and (b) thin solid films, and (c) energy level diagrams of the polymer donors and ITIC acceptor.

absorption band at about 350–500 nm is attributed to the p–p* transitions of the donor units. Especially, it can be seen that all the polymers exhibit significant shoulder peaks both in solution and film, indicating the existence of strong aggregation and p-p* stacking. Evidently, there is no change in the absorption band-gap in solution, but differences are observed in the solid-state spectra for these polymers, which are attributed to the different stacking states in solution and solid state. As we know, compared with solid states, the molecular stacking state can be weaker for the three polymers in very dilute solution. However, for the polymers with three different bulky side chains, the stacking is compact and the distances are distinct in the solid state, resulting in different band-gaps. In the solid state, the absorption peaks of $PTBFS_{EH}$-BDD and $PTBFS_{DO}$-BDD are 10 nm red-shifted than that of $PTBF_{EH}$-BDD, which is attributed to the stronger electron-donating ability of the alkylthio group than that of the alkyl group. From the solution to the solid state, a slight red-shift in the maximum absorption is also found for all the polymers, which is ascribed to the increased inter-molecular interactions. In addition, the three polymers show high molar extinction coefficients in solution. The extinction coefficient of $PTBF_{EH}$-BDD is estimated to be 6.2 × 10^5 M^{-1} cm^{-1}, while the extinction coefficients of $PTBFS_{DO}$-BDD and $PTBFS_{EH}$-BDD are slightly lower at 5.0×10^5 and 4.5 × 10^5 M^{-1} cm^{-1}, respectively, which might be caused by the reduced oscillator strengths that express the probability of absorption or emission of electromagnetic radiation during transitions between the energy levels of the molecules, and also the decreased free electron density. The temperature-dependent UV-vis absorption spectra of $PTBF_{EH}$-BDD, $PTBFS_{DO}$-BDD and $PTBFS_{EH}$-BDD were measured to further investigate the aggregation behaviors in dilute solutions (Fig. S2†). When the temperature increased to 100 ℃, the aggregation of $PTBF_{EH}$-BDD almost broke. In contrast, the solution of the

$PTBFS_{DO}$-BDD polymer still exhibits distinct shoulder peak in the long wavelength region, even if the temperature is increased to 100 ℃, indicating much stronger aggregation and intermolecular stacking even in a hot dilute solution. The optical band gaps of $PTBF_{EH}$-BDD, $PTBFS_{DO}$-BDD and $PTBFS_{EH}$-BDD are estimated to be 1.80 and 1.75 and 1.75 eV respectively, which are complementary with ITIC absorption spectrum, suggesting that high J_{SC} can be obtained in PSCs.

Electrochemical properties

Cyclic voltammetry was performed to evaluate the highest occupied molecular orbital (HOMO) and the lowest unoccupied molecular orbital (LUMO) levels (Fig. S3†).[59] The corresponding data are collected in Table 2. Fig. 1c shows the energy level diagrams of the polymers and ITIC for a clear comparison. The HOMO energy level of $PTBFS_{EH}$-BDD is estimated to be at —5.32 eV, which is 0.06 eV lower than that of $PTBF_{EH}$-BDD (—5.26 eV). The lower HOMO energy level is due to the alkylthio side chain with a weaker electron-donating ability. The HOMO energy level of $PTBFS_{DO}$-BDD was at —5.31 eV, slightly higher than that of $PTBFS_{EH}$-BDD, which meant that the branched side chain substituent on the TBF backbone could decrease the energy level compared with the linear side chain. The lower E_{HOMO} of the polymer donor is beneficial for higher V_{OC} of the PSCs. The LUMO energy levels are —3.46, —3.56 and —3.57 eV for $PTBF_{EH}$-BDD, $PTBFS_{DO}$-BDD and $PTBFS_{EH}$-BDD, respectively.

Quantum mechanical calculations

The optimal molecular geometries of the three TBF-based polymers were determined by the density functional theory (DFT) calculations at the B3LYP/6-31G(d,p) level to analyze the planarity of the polymers and the effect of the electron-donating ability of the TBF unit. As can be seen (Fig. S4†), the planarity of the backbone in the three polymers is confirmed. The dihedral angles from TBF to BDD units are 8.12°, 9.12° and 0.24° for $PTBF_{EH}$-BDD, $PTBFS_{DO}$-BDD and $PTBFS_{EH}$-BDD, respectively, suggesting that the "planar" polymer backbone will yield a strong driving force to form intermolecular stacking, which is beneficial for charge transport.[29,60]

$PTBFS_{EH}$-BDD with the alkylthio side chain possesses a smaller dihedral angle between the TBF and BDD units than the other two polymers, which may be ascribed to the reduced steric hindrance in the former's structure. For the donor side, the torsion angles between the planar TBF core and the

Table 2 Optical and electrochemical properties of the three polymers

Polymers	l_{max} (nm)[a]	l_{max} (nm)[b]	l_{edge} (nm)	E_g^{opt} (eV)	HOMO (eV)[c]	LUMO (eV)[c]	HOMO (eV)[d]	LUMO (eV)[d]
$PTBF_{EH}$-BDD	617	625	688	1.80	—5.26	—3.46	—4.99	—2.35
$PTBFS_{DO}$-BDD	623	632	708	1.75	—5.31	—3.56	—5.17	—2.42
$PTBFS_{EH}$-BDD	619	633	709	1.75	—5.32	—3.57	—5.17	—2.42

[a] Measured from the dilute $CHCl_3$ solutions. [b] Measured from films on quartz cast from $CHCl_3$ solution. [c] Measured from cyclic voltammetry. [d] Theoretical data.
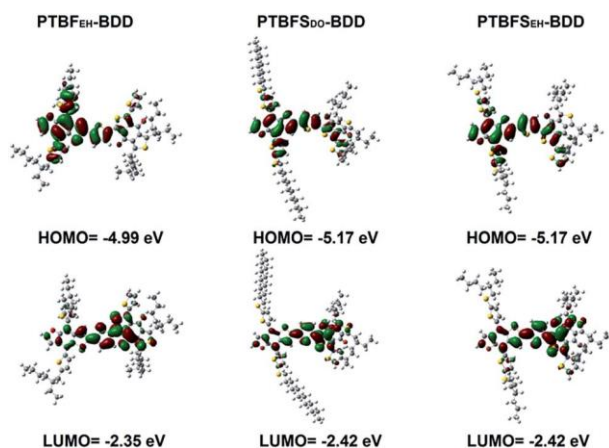
Fig. 2 Theoretical calculations on $PTBF_{EH}$-BDD, $PTBFS_{DO}$-BDD and $PTBFS_{EH}$-BDD.

Fig. 3 (a) J–V curves of $PTBF_{EH}$-BDD:ITIC, $PTBFS_{DO}$-BDD:ITIC and $PTBFS_{EH}$-BDD:ITIC based solar cells under the illumination of AM1.5G, 100 mW cm^{-2}. (b) EQE of the corresponding PSCs. (c) Photocurrent density (J_{ph}) as a function of effective voltage (V_{eff}) characteristics of the three devices under constant incident light intensity. (d) J_{ph} versus light intensity plot for the three devices.

conjugated side chain were different, ranging from 41° to 48°, much smaller than those for BDT-based polymers (57°), which may be due to the interaction of sulfur and oxygen atoms. The small torsion angles will facilitate the inter-molecular p–p* stacking interactions and crystallinity so as to increase the performance of the PTBF-based polymers. From the distribution of electron density, HOMO delocalized more on the backbone of the TBF donor units, while LUMO occupied the BDD acceptor moiety more. The diagram is shown in Fig. 2 and the theoretical data are summarized in Table 2, which are in accordance with the experimental results.

Photovoltaic properties

In order to explore the polymers' photovoltaic properties, BHJ PSCs were fabricated with a conventional structure of ITO/PEDOT:PSS/active layer/ETL/Al, with the polymer as the donor material and ITIC as the acceptor material. The devices were systematically optimized by varying the annealing temperatures, processing additives, polymer : ITIC (D : A) weight ratios, and electron transport layers (ETL). It is found that the optimal conditions for all three PTBF-based PSCs are nearly identical without any additives or annealing processes. The optimum current density–voltage (J–V) curves of the three polymers are shown in Fig. 3a and the corresponding data are summarized in Table 3. The $PTBFS_{EH}$-BDD-based PSCs show a PCE of 10.23% with a V_{OC} of 0.935 V, a J_{SC} of 17.06 mA cm^{-2}, and a FF of 64.08%. Slightly improved device performance is realized by the $PTBFS_{DO}$-BDD polymer, which exhibits a V_{OC} of 0.928 V, a FF of 66.10%, and an enhanced J_{SC} of 17.24 mA cm^{-2}, leading to a moderated PCE of 10.57%.

Compared to $PTBFS_{EH}$-BDD and $PTBFS_{DO}$-BDD, the best device performance with a PCE of 11.13% is achieved by the $PTBF_{EH}$-BDD polymer. The higher performance of $PTBF_{EH}$-BDD is mainly attributed to the slightly increased J_{SC} and larger FF (70.16%), which is probably due to the more favorable active layer blend morphology, resulting in more efficient exciton generation and superior charge carrier mobility that could promote the exciton separation and charge transportation. It is
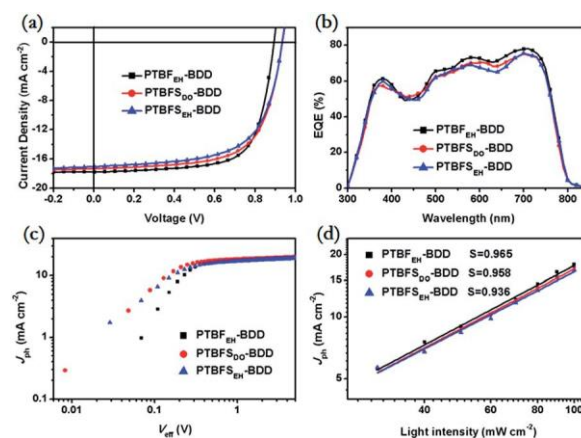
found that the subtle change in the side chains on the donor unit has a significant impact on the performance of PSCs. Additionally, the PSCs performance of a TBF-based device is highly repeatable and the device fabrication is simplified without any additives or annealing process, which is promising for future application.

From the external quantum efficiency (EQE) measurements, as shown in Fig. 3b, the $PTBF_{EH}$-BDD-based PSCs show a relatively higher photo-current response than those shown by the other two polymers, consistent with the improved J_{SC} of the respective devices. The J_{SC} values of the devices based on $PTBF_{EH}$-BDD, $PTBFS_{DO}$-BDD and $PTBFS_{EH}$-BDD are calculated from the integrations of EQE spectra to be 17.37 mA cm^{-2}, 16.87 mA cm^{-2} and 16.52 mA cm^{-2}, respectively, which is in good agreement with the values obtained from J–V measurements.

The charge transport properties also play a critical role on the photovoltaic performances of the PSCs to ensure efficient charge-carrier transport to the electrodes and to suppress the photocurrent loss by competing charge recombinations. The hole and electron mobilities were obtained by using the space charge limited current (SCLC) method. The curves and corresponding data are summarized in Fig. S5† and Table 3, respectively. The hole and electron mobility values of the as-cast $PTBF_{EH}$-BDD:ITIC blend film are found to be 2.21×10^{-4} and 2.86×10^{-4} cm^2 V^{-1} s^{-1}, respectively, with m_h/m_e ratios of 0.77, which were higher than those of $PTBFS_{DO}$-BDD:ITIC and $PTBFS_{EH}$-BDD:ITIC blend films. The higher and balanced charge transport property of the $PTBF_{EH}$-BDD:ITIC blend film was beneficial to reduce the charge recombination, which explains the high J_{SC} and FF values.[61]

Exciton dissociation efficiency (P_{diss}) was gained from the relationship between the photocurrent density (J_{ph}) and the effective voltage (V_{eff}). The value of J_{ph} is the difference between the light and dark current densities. The term V_{eff} is defined as $V_0 - V_{appl}$, where V_0 is the voltage when $J_{ph} = 0$ and V_{appl} is the applied voltage.[62,63] For the optimized device, the value of J_{ph}

reached its saturation (J_{sat}) when the value of V_{eff} was close to 2.0 V, where all the photo-generated excitons dissociate into free charges, which can be collected by the electrodes. The charge dissociation probability $P(E, T)$ is defined as the ratio of J_{ph}/J_{sat}, and is used to evaluate the exciton dissociation and charge collection efficiency. As shown in Fig. 3c, under short-circuit conditions, the J_{ph}/J_{sat} ratio for PTBF$_{EH}$-BDD:ITIC, PTBFS$_{DO}$-BDD:ITIC and PTBFS$_{EH}$-BDD:ITIC are calculated to be 92.8%, 86.2% and 85.3%, respectively, implying efficient exciton dissociation and charge collection by the three polymers. The higher J_{ph}/J_{sat} ratio of PTBF$_{EH}$-BDD:ITIC indicated a better exciton dissociation efficiency in the active layer, resulting in the high J_{SC} and FF in the optimized device. Furthermore, the correlation between J_{SC} and light intensity is fitted according to the equation $J_{ph} \propto P^S$, where S value of the fitted line is close to 1 when all the free carriers are swept out and collected with negligible bimolecular recombination.[63] As shown in Fig. 3d, logarithmic slopes between J_{SC} and light intensity for the devices based on PTBF$_{EH}$-BDD, PTBFS$_{DO}$-BDD and PTBFS$_{EH}$-BDD are 0.965, 0.958 and 0.936, respectively, suggesting that the bimolecular recombination processes are efficiently suppressed in the TBF-based devices. Particularly, the PTBF$_{EH}$-BDD-based PSCs show an S value closer to 1 compared to the PSCs based on PTBFS$_{DO}$-BDD and PTBFS$_{EH}$-BDD. These results correlate well with the relatively higher J_{SC} and FF observed for the PTBF$_{EH}$-BDD-based device. Fig. S6† shows the PL spectra of the pure polymer films and polymer:ITIC blend films. According to the absorption spectra, excitation wavelengths in the PL measurements are selected to be 570 nm for the polymer donors and 720 nm for the ITIC acceptor. Notably, the PTBF$_{EH}$-BDD:ITIC blend film shows a higher photoluminescence (PL) quenching efficiency compared to those of the PTBFS$_{DO}$-BDD:ITIC and PTBFS$_{EH}$-BDD:ITIC blend films, indicating that the polymer PTBF$_{EH}$-BDD possesses more efficient photo-induced exciton separation and charge transfer properties. Nevertheless, the PL emission of ITIC is completely quenched by all the TBF-based polymers, indicating effective charge transfer from the ITIC acceptor to the polymer donors.

Morphological characterization

Atomic force microscopy (AFM) was employed to further confirm the interrelation between the surface morphology and the photovoltaic property. As shown in Fig. 4a–c, rather smooth surfaces with root-mean-squared (RMS) roughness of 1.37, 1.06 and 1.63 nm are observed for PTBF$_{EH}$-BDD:ITIC, PTBFS$_{DO}$-BDD:ITIC and PTBFS$_{EH}$-BDD:ITIC, respectively. In the phase images of AFM (see Fig. 4d–f), it can be seen that the PTBF$_{EH}$-BDD:ITIC blend film exhibits a well-developed fibrillar nano phase with excellent bicontinuous interpenetrating network compared to the PTBFS$_{DO}$-BDD:ITIC and PTBFS$_{EH}$-BDD:ITIC blend films. Fig. 4(g–i) present the transmission electron microscopy (TEM) images, which reveal distinctly different films of the three polymer blends. As seen in Fig. 4g, no significant aggregation domains were observed and good miscibility was displayed in the nanometer scale between PTBF$_{EH}$-BDD and ITIC, which will be beneficial for more
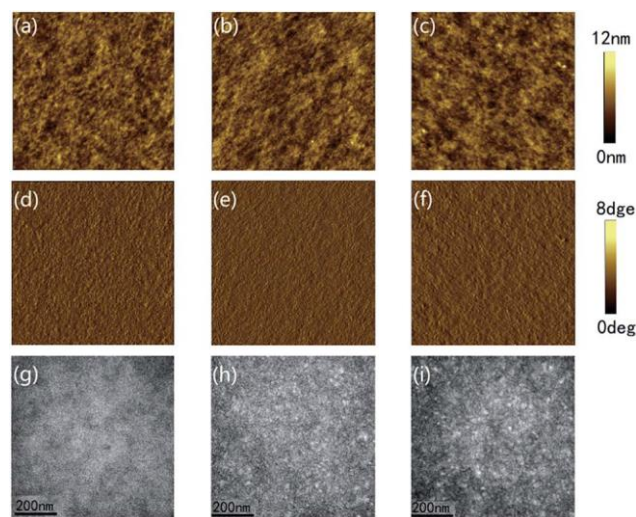

Fig. 4 AFM height images (4 mm × 4 mm) of (a) the PTBF$_{EH}$-BDD:ITIC, (b) the PTBFS$_{DO}$-BDD:ITIC and (c) the PTBFS$_{EH}$-BDD:ITIC; AFM phase images (4 mm × 4 mm) of (d) PTBF$_{EH}$-BDD:ITIC, (e) PTBFS$_{DO}$-BDD:ITIC and (f) PTBFS$_{EH}$-BDD:ITIC; TEM images of (g) PTBF$_{EH}$-BDD:ITIC, (h) PTBFS$_{DO}$-BDD:ITIC and (i) PTBFS$_{EH}$-BDD:ITIC; all blends are measured at their optimal conditions.

effective charge migration to the donor/acceptor interface for charge separation. It concurs with the result that the device based on PTBF$_{EH}$-BDD shows high J_{SC} and FF. However, conspicuous aggregation is found in the PTBFS$_{DO}$-BDD:ITIC and PTBFS$_{EH}$-BDD:ITIC blend films, which is probably due to the sulfur atoms in the side chains with strong non-covalent S–H and S–O interactions, resulting in strong aggregation of the polymers. The poor interconnectivity and miscibility of the PTBFS$_{DO}$-BDD:ITIC and PTBFS$_{EH}$-BDD:ITIC blend films observed in the TEM images would affect the charge separation and transport, leading to relatively low FF.

The molecular stacking, distances and orientations in the film state can efficiently affect the photovoltaic properties. In order to elucidate the relationship between the morphological information and the photovoltaic parameters, the microstructural features of these polymer:ITIC blend films were investigated by 2D grazing-incidence wide-angle X-ray scattering (2D GIWAXS) method. As seen in Fig. 5, for the blends at optimal
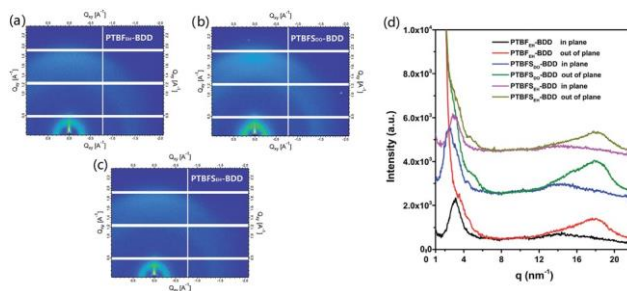

Fig. 5 (a–c) 2D GIWAXS patterns of the blended films of PTBF$_{EH}$-BDD, PTBFS$_{DO}$-BDD and PTBFS$_{EH}$-BDD, and (d) the corresponding in-plane and out-of-plane line-cut profiles for the three blends.

962 | J. Mater. Chem. A, 2019, 7, 958–964

This journal is © The Royal Society of Chemistry 2019

Table 3 The photovoltaic parameters and mobilities of the optimal devices

Blend active layer	V_{OC} (V)	J_{SC} (mA cm^{-2})	EQE J_{SC} (mA cm^{-2})	FF (%)	PCE (%)	m_h (cm^2 V^{-1} s^{-1})	m_e (cm^2 V^{-1} s^{-1})
PTBF$_{EH}$-BDD:ITIC	0.893	17.76	17.37	70.16	11.13	2.21×10^{-4}	2.86×10^{-4}
PTBFS$_{DO}$-BDD:ITIC	0.928	17.24	16.87	66.10	10.57	1.08×10^{-4}	2.37×10^{-4}
PTBFS$_{EH}$-BDD:ITIC	0.935	17.06	16.52	64.08	10.23	0.95×10^{-4}	2.63×10^{-4}

condition, the p–p (010) stacking diffraction mainly appears along the out-of-plane (OOP) direction for all three films and the corresponding (100) stacking is in the in-plane (IP) direction, indicating predominant face-on orientation in the blended films, which may benefit charge transport in our PSCs. It can be found that significantly stronger (100) peak intensities of PTBF$_{EH}$-BDD:ITIC, PTBFS$_{DO}$-BDD:ITIC and PTBFS$_{EH}$-BDD:ITIC are recorded at q_{xy} z 3.13, 2.47 and 2.98 nm^{-1}, respectively, corresponding to lamellar distances of 20.06, 25.42 and 21.07 Å, respectively, which suggest that the bulky alkyl chains on the TBF unit can result in an increase in the interchain distance and the inserted sulfur atom can also slightly increase the interchain distance of polymers. The crystal coherence lengths (CCL) in this direction are estimated to be 5.4, 7.12 and 6.46 nm for PTBF$_{EH}$-BDD:ITIC, PTBFS$_{DO}$-BDD:ITIC and PTBFS$_{EH}$-BDD:ITIC, respectively, using the Scherrer equation. The PTBFS$_{DO}$-BDD:ITIC and PTBFS$_{EH}$-BDD films exhibit high crystallinity and may be prone to excessive aggregation, which accounts for the reduced FF and PCE, and these results are in accordance with the TEM measurements. Notably, the (010) peak for PTBF$_{EH}$-BDD:ITIC is observed at q_z z 17.92 nm^{-1}, corresponding to the p–p stacking distance of z 3.53 Å, which is slightly smaller than those for the PTBFS$_{DO}$-BDD:ITIC (3.60 Å) and PTBFS$_{EH}$-BDD:ITIC (3.56 Å) films. This could increase the intermolecular charge transport in the vertical direction. The shorter p–p stacking distances are favorable for higher charge carrier mobility and consequently, the PBDF$_{EH}$-BDD-based device show the highest J_{SC} and PCE.

Conclusions

In conclusion, three two-dimensional conjugated polymers, PTBF$_{EH}$-BDD, PTBFS$_{DO}$-BDD and PTBFS$_{EH}$-BDD, based on thieno[2,3-f]benzofuran (TBF) building block with side-chain engineering, are designed and synthesized. It is found that the TBF backbone can inherit and integrate the advantages of both the BDT and BDF building blocks. When blended with ITIC, the TBF-based polymer/ITIC blended films predominantly exhibited face-on orientation. Due to the synergistic effects of the side-chain and backbone engineering, PTBF$_{EH}$-BDD shows a higher absorption coefficient, more suitable aggregation and improved hole mobility in comparison with the PTBFS$_{DO}$-BDD and PTBFS$_{EH}$-BDD blends, which improves the J_{SC} and FF in PSCs. As a result, the PSCs based on PTBF$_{EH}$-BDD:ITIC achieve a high power conversion efficiency of 11.13% with a J_{SC} of 17.76 mA cm^{-2}, V_{OC} of 0.893 V, and a FF of 70.16%, which is comparable with its BDT counterparts. The PSCs based on the three TBF-based devices do not need any extra post treatments or additives, which is very beneficial to practical applications. Our results provide new insights into the relationship between the structural and photovoltaic properties for rationally designing high-performance organic photovoltaic materials using the synergistic effects of the alkyl side-chain and backbone engineering.

Conflicts of interest

There are no conflicts to declare.

Acknowledgements

Notes and references

1 J. Hou, O. Inganäs, R. H. Friend and F. Gao, *Nat. Mater.*, 2018, 17, 119–128.
2 P. Cheng, G. Li, X. Zhan and Y. Yang, *Nat. Photonics*, 2018, 12, 131–142.
3 Z. Liu, Y. Wu, Q. Zhang and X. Gao, *J. Mater. Chem. A*, 2016, 4, 17604–17622.
4 G. Zhang, G. Yang, H. Yan, J. H. Kim, H. Ade, W. Wu, X. Xu, Y. Duan and Q. Peng, *Adv. Mater.*, 2017, 29, 1606054.
5 W. Zhao, D. Qian, S. Zhang, S. Li, O. Inganäs, F. Gao and J. Hou, *Adv. Mater.*, 2016, 28, 4734–4739.
6 H. Bin, L. Gao, Z. G. Zhang, Y. Yang, Y. Zhang, C. Zhang, S. Chen, L. Xue, C. Yang, M. Xiao and Y. Li, *Nat. Commun.*, 2016, 7, 13651.
7 X. Bao, Y. Zhang, J. Wang, D. Zhu, C. Yang, Y. Li, C. Yang, J. Xu and R. Yang, *Chem. Mater.*, 2017, 29, 6766–6771.
8 Y. Lin, J. Wang, Z. G. Zhang, H. Bai, Y. Li, D. Zhu and X. Zhan, *Adv. Mater.*, 2015, 27, 1170–1174.
9 X. Li, H. Huang, H. Bin, Z. Peng, C. Zhu, L. Xue, Z.-G. Zhang, Z. Zhang, H. Ade and Y. Li, *Chem. Mater.*, 2017, 29, 10130–10138.
10 S. Dai, F. Zhao, Q. Zhang, T. Lau, T. Li, K. Liu, Q. Ling, C. Wang, X. Lu, W. You and X. Zhan, *J. Am. Chem. Soc.*, 2017, 139, 1336–1343.
11 J. Wang, J. Zhang, Y. Xiao, T. Xiao, R. Zhu, C. Yan, Y. Fu, G. Lu, X. Lu, S. R. Marder and X. Zhan, *J. Am. Chem. Soc.*, 2018, 140, 9140–9147.
12 X. Xu, T. Yu, Z. Bi, W. Ma, Y. Li and Q. Peng, *Adv. Mater.*, 2018, 30, 1703973.
13 Z. Luo, H. Bin, T. Liu, Z.-G. Zhang, Y. Yang, C. Zhong, B. Qiu, G. Li, W. Gao, D. Xie, K. Wu, Y. Sun, F. Liu, Y. Li and C. Yang, *Adv. Mater.*, 2018, 30, 1706124.

This journal is © The Royal Society of Chemistry 2019

J. Mater. Chem. A, 2019, 7, 958–964 | 963

14 D. Xie, T. Liu, W. Gao, C. Zhong, L. Huo, Z. Luo, K. Wu, W. Xiong, F. Liu, Y. Sun and C. Yang, *Sol. RRL*, 2017, 1, 1700044.

15 Y. Li, J. D. Lin, X. Che, Y. Qu, F. Liu, L. S. Liao and S. R. Forrest, *J. Am. Chem. Soc.*, 2017, 139, 17114–17119.

16 Z. Fei, F. D. Eisner, X. Jiao, M. Azzouzi, J. A. Rohr, Y. Han, M. Shahid, A. S. R. Chesman, C. D. Easton, C. R. McNeill, T. D. Anthopoulos, J. Nelson and M. Heeney, *Adv. Mater.*, 2018, 30, 1705209.

17 M. Jeong, S. Chen, S. M. Lee, Z. Wang, Y. Yang, Z.-G. Zhang, C. Zhang, M. Xiao, Y. Li and C. Yang, *Adv. Energy Mater.*, 2017, 1702166.

18 C. Sun, F. Pan, H. Bin, J. Zhang, L. Xue, B. Qiu, Z. Wei, Z.-G. Zhang and Y. Li, *Nat. Commun.*, 2018, 9, 743.

19 W. Liu, J. Zhang, Z. Zhou, D. Zhang, S. Xu and X. Zhu, *Adv. Mater.*, 2018, 30, 1800403.

20 Z. Xiao, X. Jia and L. Ding, *Sci. Bull.*, 2017, 62, 1562–1564.

21 S. Zhang, Y. Qin, J. Zhu and J. Hou, *Adv. Mater.*, 2018, 30, 1800868.

22 S. Li, L. Ye, W. Zhao, H. Yan, B. Yang, D. Liu, W. Li, H. Ade and J. Hou, *J. Am. Chem. Soc.*, 2018, 140, 7159–7167.

23 T. Liu, Z. Luo, Q. Fan, G. Zhang, L. Zhang, W. Gao, X. Guo, W. Ma, M. Zhang, C. Yang, Y. Li and H. Yan, *Energy Environ. Sci.*, 2018, 11, 3275–3282.

24 X. Che, Y. Li, Y. Qu and S. R. Forrest, *Nat. Energy*, 2018, 3, 422–427.

25 Y. Zhang, B. Kan, Y. Sun, Y. Wang, R. Xia, X. Ke, Y. Q. Q. Yi, C. Li, H. L. Yip, X. Wan, Y. Cao and Y. Chen, *Adv. Mater.*, 2018, 30, 1707508.

26 Q. Fan, W. Su, X. Guo, Y. Wang, J. Chen, C. Ye, M. Zhang and Y. Li, *J. Mater. Chem. A*, 2017, 5, 9204–9209.

27 T. Liu, X. Pan, X. Meng, Y. Liu, D. Wei, W. Ma, L. Huo, X. Sun, T. H. Lee, M. Huang, H. Choi, J. Y. Kim, W. C. Choy and Y. Sun, *Adv. Mater.*, 2017, 29, 1604251.

28 Z. G. Zhang and Y. Li, *Sci. China: Chem.*, 2015, 58, 192–209.

29 D. Zhu, X. Bao, Q. Zhu, C. Gu, M. Qiu, S. Wen, J. Wang, B. Shahid and R. Yang, *Energy Environ. Sci.*, 2017, 10, 614–620.

30 Y. Yang, Z. G. Zhang, H. Bin, S. Chen, L. Gao, L. Xue, C. Yang and Y. Li, *J. Am. Chem. Soc.*, 2016, 138, 15011–15018.

31 D. Liu, J. Wang, C. Gu, Y. Li, X. Bao and R. Yang, *Adv. Mater.*, 2018, 30, 1705870.

32 G. Zhang, X. Xu, Z. Bi, W. Ma, D. Tang, Y. Li and Q. Peng, *Adv. Funct. Mater.*, 2018, 28, 1706404.

33 P. Gao, J. Tong, P. Guo, J. Li, N. Wang, C. Li, X. Ma, P. Zhang, C. Wang and Y. Xia, *J. Polym. Sci., Part A: Polym. Chem.*, 2018, 56, 85–95.

34 Y. Wu, Z. Li, W. Ma, Y. Huang, L. Huo, X. Guo, M. Zhang, H. Ade and J. Hou, *Adv. Mater.*, 2013, 25, 3449–3455.

35 B. Qiu, R. Cui, J. Yuan, H. Peng, Z. Zhang, Y. Li and Y. Zou, *Phys. Chem. Chem. Phys.*, 2015, 17, 17592–17600.

36 Y. Gao, Z. Wang, J. Zhang, H. Zhang, K. Lu, F. Guo, Y. Yang, L. Zhao, Z. Wei and Y. Zhang, *J. Mater. Chem. A*, 2018, 6, 4023–4031.

37 X. Wang, Q. Su, Y. Li, C. Cheng, Y. Xia, L. He, H. Li, G. Shu and F. Wang, *Synth. Met.*, 2016, 220, 433–439.

38 Y. Wu, C. An, L. Shi, L. Yang, Y. Qin, N. Liang, C. He, Z. Wang and J. Hou, *Angew. Chem., Int. Ed.*, 2018, 57, 12911–12915.

39 H. Yao, L. Ye, H. Zhang, S. Li, S. Zhang and J. Hou, *Chem. Rev.*, 2016, 116, 7397–7457.

40 H. Yao, L. Ye, J. Hou, B. Jang, G. Han, Y. Cui, G. M. Su, C. Wang, B. Gao, R. Yu, H. Zhang, Y. Yi, H. Y. Woo, H. Ade and J. Hou, *Adv. Mater.*, 2017, 29, 1700254.

41 F. Liu, W. Zhao, J. R. Tumbleston, C. Wang, Y. Gu, D. Wang, A. L. Briseno, H. Ade and T. P. Russell, *Adv. Energy Mater.*, 2014, 4, 1301377.

42 L. Huo, T. Liu, B. Fan, Z. Zhao, X. Sun, D. Wei, M. Yu, Y. Liu and Y. Sun, *Adv. Mater.*, 2015, 27, 6969–6975.

43 X. Chen, B. Liu, Y. Zou, L. Xiao, X. Guo, Y. He and Y. Li, *J. Mater. Chem.*, 2012, 22, 17724–17731.

44 P. Huang, J. Du, M. C. Biewer and M. Stefan, *J. Mater. Chem. A*, 2015, 3, 6244–6257.

45 O. Gidron, Y. Diskin-Posner and M. Bendikov, *J. Am. Chem. Soc.*, 2010, 132, 2148–2150.

46 Y. Zhang, L. Gao, C. He, Q. Sun and Y. Li, *Polym. Chem.*, 2013, 4, 1474–1481.

47 L. Huo, L. Ye, Y. Wu, Z. Li, X. Guo, M. Zhang, S. Zhang and J. Hou, *Macromolecules*, 2012, 45, 6923–6929.

48 L. Ye, S. Zhang, W. Zhao, H. Yao and J. Hou, *Chem. Mater.*, 2014, 26, 3603–3605.

49 H. Hu, K. Jiang, G. Yang, J. Liu, Z. Li, H. Lin, Y. Liu, J. Zhao, J. Zhang, F. Huang, Y. Qu, W. Ma and H. Yan, *J. Am. Chem. Soc.*, 2015, 137, 14149–14157.

50 X. Wang, J. Tong, P. Guo, Y. Li, H. Li, Y. Xia and F. Wang, *Polymer*, 2017, 122, 96–104.

51 C. Cui, W. Y. Wong and Y. Li, *Energy Environ. Sci.*, 2014, 7, 2276–2284.

52 L. Qiu, J. Yuan, D. He, Z.-G. Zhang, Y. Li and Y. Zou, *Dyes Pigm.*, 2017, 140, 337–345.

53 D. He, L. Qiu, J. Yuan, Z.-G. Zhang, Y. Li and Y. Zou, *Polymer*, 2017, 114, 348–354.

54 L. Qiu, H. Peng, Y. Liu, B. Qiu, Z. Zhang, Y. Li and Y. Zou, *Org. Electron.*, 2017, 45, 42–48.

55 Y. Gao, R. Zhu, Z. Wang, F. Guo, Z. Wei, Y. Yang, L. Zhao and Y. Zhang, *ACS Appl. Energy Mater.*, 2018, 1, 1888–1892.

56 L. Han, W. Chen, T. Hu, J. Ren, M. Qiu, Y. Zhou, D. Zhu, N. Wang, M. Sun and R. Yang, *ACS Macro Lett.*, 2015, 4, 361–366.

57 L. Han, H. Jiang, D. Ouyang, W. Chen, T. Hu, J. Wang, S. Wen, M. Sun and R. Yang, *Nano Energy*, 2017, 36, 110–117.

58 K. Feng, G. Yang, X. Xu, G. Zhang, H. Yan, O. Awartani, L. Ye, H. Ade, Y. Li and Q. Peng, *Adv. Energy Mater.*, 2017, 1602773.

59 C. M. Cardona, W. Li, A. E. Kaifer, D. Stockdale and G. C. Bazan, *Adv. Mater.*, 2011, 23, 2367–2371.

60 Z. Li, H. Lin, K. Jiang, J. Carpenter, Y. Li, Y. Liu, H. Hu, J. Zhao, W. Ma, H. Ade and H. Yan, *Nano Energy*, 2015, 15, 607–615.

61 W. Li, S. Albrecht, L. Yang, S. Roland, J. R. Tumbleston, T. McAfee, L. Yan, M. A. Kelly, H. Ade, D. Neher and W. You, *J. Am. Chem. Soc.*, 2014, 136, 15566–15576.

62 P. W. M. Blom, V. D. Mihailetchi, L. J. A. Koster and D. E. Markov, *Adv. Mater.*, 2007, 19, 1551–1566.

63 C. M. Proctor, M. Kuik and T.-Q. Nguyen, *Prog. Polym. Sci.*, 2013, 38, 1941–1960.